Axo-glial Dysjunction

A Novel Structural Lesion That Accounts for Poorly Reversible Slowing of Nerve Conduction in the Spontaneously Diabetic Bio-Breeding Rat

Anders A. F. Sima, Sarah A. Lattimer, Soroku Yagihashi, and Douglas A. Greene
Section of Neuropathology, Department of Pathology, University of Manitoba Faculty of Medicine, Winnipeg MB Canada R3E 0W3; and The Diabetes Research Laboratories, Department of Medicine, School of Medicine, University of Pittsburgh, Pittsburgh, Pennsylvania 15261

Abstract

Biochemical abnormalities in peripheral nerve are thought to precede and condition the development of diabetic neuropathy, but metabolic intervention in chronic diabetic neuropathy produces only limited acute clinical response. The residual, metabolically unresponsive neurological deficits have never been rigorously defined in terms of either persistent metabolic derangements or irreversible structural defects because (*a*) human nerve tissue is rarely accessible for anatomical and biochemical study and (*b*) experimentally diabetic animals do not develop the structural hallmarks of human diabetic neuropathy. Detailed neuroanatomical-functional-biochemical correlation was therefore undertaken in long-term spontaneously diabetic BB-Wistar rats that functionally and structurally model human diabetic neuropathy. Vigorous insulin replacement in chronically diabetic BB rats essentially normalized both the sural nerve fiber caliber spectrum and the decreased sciatic nerve myo-inositol and (Na,K)-ATPase levels generally associated with conduction slowing in diabetic animals; yet, nerve conduction was only partially restored toward normal. Morphometric analysis revealed a striking disappearance of paranodal axo-glial junctional complexes that was not corrected by insulin replacement. Loss of these strategic junctional complexes, which are thought to limit lateral migration of axolemmal Na channels away from nodes of Ranvier, correlates with and can account for the diminished nodal Na permeability and resultant nodal conduction delay characteristic of chronic diabetic neuropathy in this animal model.

Introduction

Diabetic neuropathy reflects a complex interplay between disturbances in nerve metabolism induced by chronic insulin deficiency and/or hyperglycemia, and undefined independent genetic and/or environmental factors. Readily reversible defects in nerve metabolism in the diabetic rat directly contribute to reversible conduction slowing resembling that of early human diabetes (1, 2). Although similar metabolic disturbances presumably condition the development of symptomatic neuropathy in susceptible diabetic patients, metabolic intervention produces only limited electrophysiologic or clinical response once diabetic neuropathy is clinically established (3, 4). The structural and/or biochemical lesions responsible for poorly reversible neurological deficits in diabetic patients, and the role of antecedent reversible functional and metabolic abnormalities in their development, remain unclear. The spontaneously diabetic BB rat exhibits both reversible nerve conduction slowing and subsequent structural lesions characteristic of human diabetic neuropathy (5–7). It thereby provides a unique model in which to explore interrelationships between readily reversible and poorly reversible metabolic, functional and structural defects in diabetic peripheral nerve (5–7).

Recent studies attribute nerve conduction slowing in diabetic rats to alterations in nerve Na and Na-related metabolism (8–11). In the experimentally diabetic rodent, increased extracellular glucose concentration reduces nerve myo-inositol (MI)[1] content by competitive inhibition of Na-gradient-dependent MI uptake and/or increased polyol (sorbitol) pathway activity (8, 12, 13). Nerve MI depletion in turn impairs nerve (Na,K)-ATPase (9, 14, 15), probably via decreased protein kinase C activity reflecting diminished intracellular diacylglycerol and/or inositol-1,4,5-triphosphate release from inositol phospholipids (16). Single-node voltage-clamp experiments in the acutely diabetic BB-Wistar rat ascribe the earliest and most readily reversible conduction slowing to a diminished nodal Na equilibrium potential attributable to impaired axonal (Na,K)-ATPase activity that selectively blocks conduction in the largest and most rapidly conducting myelinated nerve fibers (10, 11). Accompanying histologically demonstrated paranodal nerve fiber swelling has been attributed to elevated axonal Na concentrations (17, 18). These electrophysiological and structural abnormalities are completely reversed by vigorous insulin treatment within the first 3 wk of diabetes (17, 18). More prolonged hyperglycemia further slows nerve conduction by decreasing maximal nodal Na permeability (17, 18) by an unknown mechanism. Vigorous insulin treatment initiated 3 mo after the onset of diabetes in the BB rat completely corrects nerve MI content and (Na,K)-ATPase activity (and presumably the axolemmal Na-gradient), but nerve conduction velocity is only partially restored (15). Therefore, additional poorly reversible structural and/or metabolic defects, possibly associated with persistently reduced nodal Na permeability, have been postulated (15). The studies reported here examine nerve conduction, biochemistry, and morphometry in insulin-deficient and insulin-replaced chronically diabetic BB-Wistar rats with persistent slowing of nerve conduction. Nodes of Ranvier in large myelinated fibers were particularly scrutinized in an attempt to identify a structural basis for the persistently reduced nodal Na permeability thought to be responsible for poorly reversible conduction slowing in this animal model (17, 18). Although the nerve fiber caliber spectrum in the insulin-replaced diabetics was virtually completely normalized, newly described structural

Received for publication 21 May 1985.

J. Clin. Invest.

0021-9738/86/02/0474/11 $1.00
Volume 77, February 1986, 474–484

1. *Abbreviations used in this paper:* EMPA, amplitude of the evoked muscle potential; MI, myo-inositol; MNCV, motor nerve conduction velocity; PZI, protamine zinc insulin.

Table I. Characteristics of Nondiabetic Control Rats and the Three Diabetic Groups at Entry into the Study Protocol

Animal groups		Age	Body wt	Blood glucose	Urine volume	MNCV	EMPA
	n	*d*	*g*	*mg/dl*	*ml/d*	*m/s*	*mV*
Nondiabetic controls	10	201±6	488±16	85±9	10±2	52.8±0.7	4.5±0.1
Insulin-deficient diabetics	8	202±7	439±14*	343±33‡	66±7‡	40.6±0.9‡	3.0±0.2‡
Insulin-replaced diabetics	8	201±5	444±10*	341±42‡	62±6‡	38.8±0.7‡	3.0±0.1‡
Baseline diabetics	5	205±7	441±12*	361±24‡	67±13‡	40.1±1.1‡	2.8±0.3‡

Prediabetic BB-Wistar rats developed spontaneous diabetes at age 104±6 d, and were thereafter maintained persistently hyperglycemic for 12 wk on small daily doses of PZI insulin (0.5–3.0 U) until entry into the study protocol, at which time the above data were collected. At entry, diabetic rats were assigned in matched triplets to one of three groups: baseline diabetics were studied electrophysiologically as described in Methods, and then killed immediately for morphological studies. Insulin-deficient diabetics were studied electrophysiologically and then maintained hyperglycemic on small doses of PZI for the 6-wk study protocol. Insulin-replaced diabetics were begun on vigorous insulin treatment designed to normalize blood glucose values as described in Methods, Table II, and Fig. 2. * $P < 0.05$ vs. nondiabetic controls. ‡ $P < 0.001$ vs. nondiabetic control.

abnormalities of the paranodal axon-myelin junctional apparatus persisted, and correlated closely with poorly reversible conduction slowing in these chronically diabetic BB rats.

Methods

Experimental design and animal model. Prediabetic male BB rats obtained from Health and Welfare Canada, Ottawa, Canada (courtesy of Dr. P. Thibert), and age-matched nondiabetic male Wistar rats were maintained in individual air-filtered metabolic cages with ad lib. access to water and rat chow (Wayne Lab Blox F-6, Wayne Laboratory Animal Diets, Wayne Feed Div., Winnipeg, Manitoba, Canada [MI content 0.022% wt/wt]). Body weight, urine volume, and glucosuria (Testape; Eli Lilly Canada, Inc., Toronto, Ontario, Canada) were monitored daily, and glucose was measured in tail-vein blood samples by Ames Eyetone (Miles Laboratory, Ltd., Rexdale, Ontario, Canada) every second day between 2 and 4 p.m. 12 wk after onset of diabetes, age-matched triplets of diabetic animals were randomly distributed into three groups: baseline diabetics were killed immediately in order to obtain baseline structural and morphometric parameters; insulin-deficient diabetics were continued for 6 wk on small daily doses (0.5–3.0 U/d) of protamine zinc insulin (PZI) (Connaught Laboratories, Ltd., Toronto, Ontario, Canada) designed to maintain blood glucose levels between 350 and 450 mg/dl; insulin-replaced diabetics were treated aggressively with PZI doses (3.0–6.0 U/d) adjusted for changes in blood glucose for 6 wk in order to achieve and maintain euglycemia. All end-point measurements (nerve conduction, morphological and biochemical assessments) were performed by investigators who were unaware of the identity of the examined material.

Electrophysiological studies. Animals were lightly anesthetized with ethyl ether (Fisher Scientific Co., Fair Lawn, NJ). Motor nerve conduction velocity (MNCV) was determined noninvasively in the sciatic-posterior tibial conduction system in a temperature-controlled environment as previously described in detail (19). Briefly, the left sciatic-tibial nerve was stimulated proximally at the sciatic notch and distally at the ankle via bipolar electrodes using supramaximal stimuli (8 V) from a Tektronix TM 501 stimulator (Tektronix, Inc., Beaverton, OR) at 20 Hz. Evoked muscle potential amplitudes (EMPA) were collected from the first interosseous space of the hindpaw by a unipolar platinum recording electrode and displayed on a Tektronix 511 storage oscilloscope. MNCV was calculated by subtracting the distal from the proximal latency measured in milliseconds from stimulus artifact to take off of the evoked muscle potential; the resultant difference was divided into the distance between the stimulating electrodes measured in millimeters, yielding a value for MNCV in meters per second. MNCV and EMPA were measured on a weekly basis throughout the study.

Tissue and blood collection. On the day after the final MNCV determination, nonfasted animals were anesthetized with Na pentobarbital (50 mg/kg body weight). Midthigh segments of the left and right sciatic nerves were surgically removed, weighed, and processed either for en-

Table II. Effect of Prolonged Insulin Deficiency and Short-term Insulin Replacement on Growth, Hyperglycemia, and Nerve Conduction during the Study Protocol

Animal groups		Age	Attained body wt	Blood glucose	Urine volume	MNCV	EMPA	Nerve MI	Nerve (Na,K)-ATPase
	n	*d*	*g*	*mg/dl*	*ml/d*	*m/s*	*mV*	*mmol/kg*	*μmol/g/h*
Nondiabetic controls	10	247±5	563±20	135±12	10±2	52.8±0.6	4.9±0.1	3.02±0.26	117.0±9.8
Insulin-deficient diabetics	8	243±4	433±13*	480±13*	72±6*	40.0±0.4*	3.0±0.1*	2.19±0.15‡	89.0±7.2§
Insulin-replaced diabetics	8	243±4	518±16‖	140±21‖	17±3‖	47.1±0.5*‖	4.7±0.1‖	3.18±0.18‖	121.4±7.6¶

After 12-wk of insulin deficiency, diabetic rats were either continued hyperglycemic on small daily doses of PZI (insulin-deficient diabetics) or given insulin replacement therapy designed to normalize blood glucose (insulin-replaced diabetics) during the 6-wk study protocol as described in Methods and in Table I. Data were collected on the last day of the study protocol, after either 18 wk of insulin deficiency (insulin-deficient diabetics) or 12 wk of insulin deficiency followed by 6 wk of insulin replacement (insulin-replaced diabetics). (Na,K)-ATPase activity was assessed enzymatically in crude homogenates of sciatic nerve by comparing total ATPase activity in the presence and absence of Na and K ions as summarized in Methods and previously described in detail (9). Similar values for (Na,K)-ATPase were obtained in these same nerve homogenates by comparing ATPase activity in the presence and absence of 0.10 mM ouabain (15). These were published separately in detail (15) and are summarized here for comparison only. * $P < 0.001$ vs. nondiabetic controls. ‡ $P < 0.01$ vs. nondiabetic controls. § $P < 0.01$ vs. insulin-deficient diabetics. ‖ $P < 0.001$ vs. insulin-deficient diabetics. ¶ $P < 0.01$ vs. insulin-deficient diabetics.

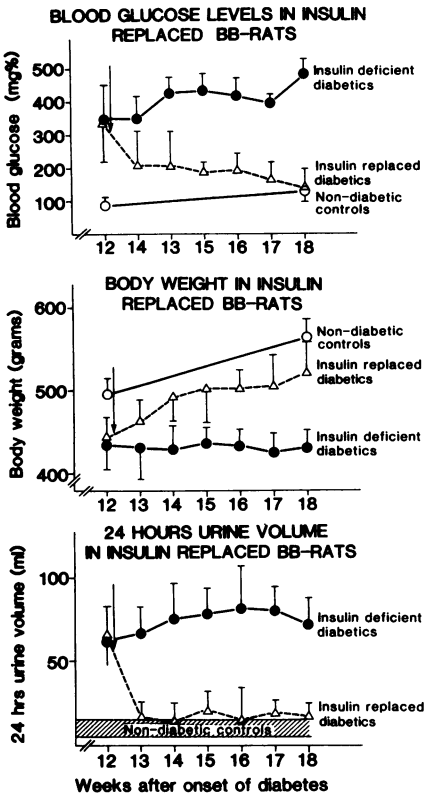

Figure 1. Effects of insulin deficiency and insulin replacement on hyperglycemia and growth in spontaneously diabetic BB-Wistar rats. After being maintained hyperglycemic and polyuric for 12 wk on small daily doses of insulin, BB-Wistar rats were divided into two treatment groups for the remaining 6 wk of the study protocol: insulin-deficient diabetics (solid lines, closed circles) were continued hyperglycemic on small daily doses of insulin, and insulin-replaced diabetics (broken lines, open triangles) were given larger replacement doses of insulin adjusted according to blood glucose measurements to achieve euglycemia as described in Methods and Tables I and II. Age- and sex-matched Wistars were used as nondiabetic controls (solid lines, open circles). Data shown here for the three subgroups (n = 5 in each) employed for morphological study did not differ significantly from those for the full groups employed for biochemical measurements at the beginning or the end of the 6-wk treatment protocol (compare with Tables I and II).

zymatic ATPase measurements or for gas-liquid chromatographic determination of MI content as previously described in detail (9). Blood was aspirated from the left ventricle for analysis of serum osmolality by freezing point depression and pH (Radiometer, Copenhagen, Denmark). The right proximal sural nerve (opposite to the side on which MNCV was performed) was fixed in situ for 10 min by a 2.5% cacodylate-buffered (pH 7.40) glutaraldehyde fixative adjusted to an osmolality of 300 mosmol with sucrose. The proximal sural nerve was then carefully dissected, left in the same fixative for 4 h at 4°C, postfixed in 1% cacodylate-buffered osmium tetroxide (pH 7.40) for 2 h, dehydrated and embedded in Epon. Fixed and embedded sural nerves from 5 of the 10 controls (numbers 1, 3, 5, 7, and 9) 5 of 8 insulin-deficient and insulin-replaced diabetics (numbers 1, 2, 4, 6, and 8), and all 5 baseline diabetics were sectioned and examined microscopically. Ultrathin cross and longitudinal sections were stained with aqueous uranyl acetate and lead citrate.

Qualitative structural examination. Longitudinal and cross-sections of the sural nerve were examined electronmicroscopically. Qualitative changes, such as malorientation of neurofilaments, glycogenosomes, polyglucosan bodies, honeycombed profiles, axonal degeneration, and Hirano bodies were quantified in 200 randomly chosen fibers from each nerve, as previously described, and their frequency was expressed in percent (7).

Quantitative morphometry: myelinated fiber size and distribution. Semi-thin (0.5 μm) toluidine-blue-stained transverse sections of the entire unifascicular sural nerve were photographed, and prints with a magnification of 1,000 times were used to calculate the area of each myelinated fiber with the aid of a 9872A digitizer interfaced with a 9825A desk computer and plotter (Hewlett-Packard Co., Cupertino, CA). Corresponding values for fiber diameters were calculated from the digitized areas, assuming the fibers were circular. The fascicular area of each nerve was digitized from photographic prints with a total magnification of 250 times. Myelinated fiber density per unit area and myelinated fiber occupancy (percent of the fascicular area occupied by myelinated fibers) were calculated as previously described (7). Axon-myelin ratio: Electronmicroscopic prints with a total magnification of 27,420 times were used to calculate the ratio between the natural logarithm of the axonal cross-sectional area and the corresponding myelin-sheath thickness expressed by the number of myelin lamellae. A mean of 47.2±3.7 fibers randomly chosen from each nerve were examined. Frequency of axo-glial junctions: 358±40 terminal myelin loops were studied in each nerve for the presence of axo-glial junctions. Only terminal loops that contained clearly discernable double-layered membranes at the apposition of the axolemma to the myelin membrane were examined. The frequency of such myelin loops without axo-glial junctions in each paranodal area was compared with fiber diameter, and the percentage of loops without junctions in each animal was compared with MNCV by linear regression analysis.

Biochemical measurements: plasma and sciatic nerve MI. Plasma and sciatic nerve MI were determined gas-liquid chromatographically in protein-free Somogyi filtrates of cardiac blood plasma or sciatic nerve

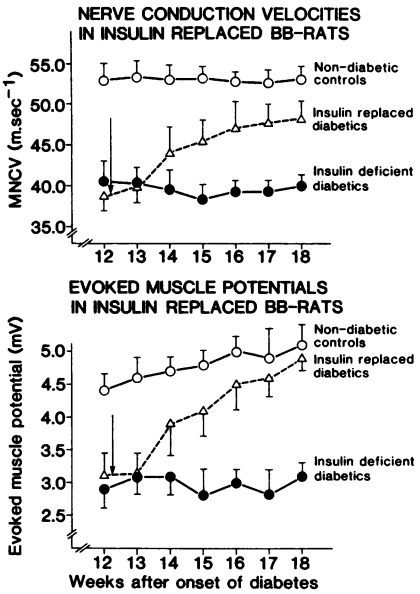

Figure 2. Effects of insulin deficiency and insulin replacement on MNCV and EMPA in spontaneously diabetic BB-Wistar rats. After 12 wk of insulin deficiency, noninvasive nerve conduction studies were performed weekly for 6 wk while diabetics were either maintained hyperglycemic (insulin-deficient diabetics: solid lines, closed circles) or were replaced with insulin to achieve euglycemia (insulin-replaced diabetics: broken lines, open triangles) as described in Methods, Tables I and II and Fig. 1. Age- and sex-matched Wistars served as nondiabetic controls (solid line, open circles). Data shown for the subgroups employed for morphological study did not differ significantly from complete groups of rats used for biochemical study either at the beginning or the end of the 6-wk treatment protocol (compare with Tables I and II).

homogenates as previously described (12, 20). (Na,K)-ATPase activity: (Na,K)-ATPase activity was measured enzymatically as (Na + K)-stimulated and ouabain-inhibited ATPase activities in freshly prepared crude homogenates of whole sciatic nerve as previously described in detail (8). Briefly, nerve segments were minced and homogenized at 4°C in 2 ml of 0.2 M sucrose-0.02 M Tris-HCl, pH 7.5. 5–20 μl of homogenate was assayed spectrophotometrically in 1 ml of 100 mM NaCl, 100 mM KCl, 2.5 mM $MgCl_2$, 1 mM Tris-ATP, 1 mM tri(cyclohexylammonium) phosphoenolpyruvate, 30 mM imidazole-HCl buffer (pH 7.3), 0.15 mM NADH, 50 μg of lactate dehydrogenase, and 30 μg of pyruvate kinase (21). (Na + K)-stimulated and ouabain-inhibited ATPase activities were computed by subtracting from this reaction rate the respective rates in the absence of NaCl and KCl or in the presence of 0.10 mM ouabain (8).

Statistics. The results are presented as mean±SEM, and significance of difference was calculated by *t* test. Linear regression analysis was performed by the method of least squares. The comparison of myelinated fiber size distribution was performed using chi-square distribution and the individual size frequencies were compared using *t* test.

Results

Development of spontaneous diabetes (Table I). Prediabetic rats (n = 21) developed diabetes at 104±6 d of age (range 89–131) and were persistently hyperglycemic (blood glucose 354±6 mg/dl, n = 21) for 89±3 d before being entered into the three experimental groups. Body weight, blood glucose, and 24-h urine volume were similarly increased in all three experimental groups at the time of random assignment, and MNCV and EMPA were similarly decreased (Table I).

Insulin replacement therapy (Table II and Fig. 1). Vigorous insulin therapy progressively lowered and, after 6 wk, normalized plasma glucose levels in the insulin-replaced diabetics (Table II, column 3), and in the subgroup of insulin-replaced diabetics that underwent morphological assessment (Fig. 1, top panel). Growth rate and 24-h urine volume were similarly normalized by insulin replacement therapy (Table II, columns 2 and 4, and Fig. 1, middle and bottom panels). Small but significant differences in plasma osmolality (312±4 mosmol in insulin-deficient diabetics vs. 282±2 mosmol in nondiabetic controls) and pH (7.29±0.02 in insulin-deficient diabetics vs. 7.39±0.02 in nondiabetic controls) were also normalized by insulin replacement (287±3 mosmol and 7.38±0.02).

Electrophysiological measurements (Table II and Fig. 2). 6 wk of insulin replacement significantly improved MNCVs and EMPAs in the insulin-replaced diabetics (Table II, columns 5 and 6) and the similarly treated subgroup that was studied morphologically (Fig. 2, top and bottom panels). MNCV remained essentially unchanged in both the nondiabetic controls and the 23% slower-conducting insulin-deficient diabetics, while increasing 21% in the insulin-replaced diabetics (compare Table I, column 5, with Table II, column 5, and see Fig. 2, top panel). However, MNCV in the insulin-replaced diabetics remained 11% below that of the nondiabetic control (Table II, column 5, and Fig. 2, top panel). In contrast, EMPA was completely normalized by 6 wk of insulin replacement (Table II, column 6, Fig. 2, bottom panel). Thus, despite insulin replacement therapy that normalized plasma glucose and growth rate in diabetic rats, MNCV was only partially restored to normal.

Nerve MI and (Na,K)-ATPase (Table II). Sciatic nerve MI in the insulin-deficient diabetics was reduced by 27% compared with the nondiabetic controls, and insulin replacement therapy raised nerve MI to that of the nondiabetic control (Table II, column 7). (Na,K)-ATPase activity, as determined by (Na + K)-stimulation (Table II, column 8) or ouabain inhibition (data not shown) was reduced 24% in the insulin-deficient diabetic compared with the nondiabetic control. Insulin replacement raised (Na,K)-ATPase activity by 34%, so that it was no longer different from the nondiabetic control (Table II, column 8). Residual ATPase activity in the presence of ouabain or in the absence of Na and K ions (i.e., non-(Na,K)-ATPase activity) was similar in all three treatment groups (data not shown). Therefore, in contrast to untreated streptozocin diabetes, spontaneous diabetes (treated with small maintenance doses of insulin) specifically influenced only (Na,K)-ATPase activity in sciatic nerve homogenates (15). However, this defect was completely corrected by vigorous insulin replacement and therefore, the persistence of slowed MNCV in the insulin-replaced diabetics could not be explained on the basis of continued abnormalities in nerve MI metabolism or (Na,K)-ATPase activity (15).

Qualitative morphology in sural nerve sections: transverse sections (Table III). Marginated maloriented neurofilaments were encountered in <1% of myelinated axons in normal controls, and >3% of myelinated fibers in baseline, insulin-replaced

*Table III. Percentage Frequency of Qualitative Structural Abnormalities in Randomly Selected Sural Nerve Myelinated Fibers**

Animal groups degeneration	Maloriented neurofilaments	Glycogenosomes	Honeycombed profiles	Axonal degeneration
	%	%	%	%
Nondiabetic controls (n = 5)	0.75±0.25	0.50±0.29	0.25±0.25	0.00±0.00
	$P < 0.005$	$P < 0.005$	$P < 0.001$	$P < 0.01$
Insulin-deficient diabetics (n = 5)	3.88±0.60	4.75±0.93	2.13±0.10	0.38±0.10
	$P < 0.025$		$P < 0.001$ $P < 0.05$	
Insulin-replaced diabetics (n = 5)	3.25±0.78	1.38±1.22	0.88±0.10	0.10±0.10
	$P < 0.001$	$P < 0.001$	$P < 0.005$ $P < 0.005$	$P < 0.05$
Baseline diabetics (n = 5)	4.60±0.57	3.88±0.60	3.25±0.60	0.26±0.10

200 randomly selected myelinated nerve fibers were examined electronmicroscopically in longitudinal and cross-sections of plastic-embedded sural nerves, and graded for the presence or absence of the structural abnormalities listed above. The observer was unaware as to the origin of the specimen at the time grading was done. * From nondiabetic controls and insulin-deficient and insulin-replaced diabetics at the completion of the study protocol, and insulin-deficient diabetics at baseline.

and insulin-deficient diabetics; this difference was highly statistically significant, and was unaffected by insulin replacement therapy (Table III, column 1). Axonal glycogenosomes and honeycombed profiles at the Schwann cell-axon interface were observed with an almost 10-fold greater frequency in insulin-deficient rats than in normal controls; insulin replacement therapy reduced these approximately threefold so that they were no longer significantly greater than the nondiabetic control (Table III, columns 2 and 4). Only rarely could acute axonal degeneration and axonal Hirano bodies be demonstrated in insulin-deficient diabetics. Persistently slowed MNCV in the insulin-replaced diabetics is not readily explicable on the basis of these qualitative structural alterations in cross-sections of sural nerves. Longitudinal sections (Fig. 3): Insulin-deficient diabetics demonstrated irregularities of paranodal myelin such as retraction of terminal myelin loops and disruption of individual myelin lamellae. Axo-glial junctional complexes between terminal myelin loops and the axolemma of myelinated axons in the regions of nodes of Ranvier were frequently absent in the insulin-deficient animals. Insulin replacement failed to normalize this abnormality, thereby providing a potential explanation for persistence of the conduction defect in the insulin-replaced diabetics (see below) (Fig. 3).

Sural nerve cross-sectional area, and myelinated fiber density and number (Table IV). There were no differences in total number of myelinated fibers, total fascicular area, or fiber density in sural nerve sections from insulin replaced, deficient, or baseline diabetics or the nondiabetic controls (Table IV).

Myelinated fiber size and distribution (Table IV, Figs. 4–7). Insulin-deficient rats exhibited a significant shift in sural nerve fiber caliber spectrum toward smaller fibers as compared with nondiabetic controls ($P < 0.005$) (Fig. 4). This shift was due to

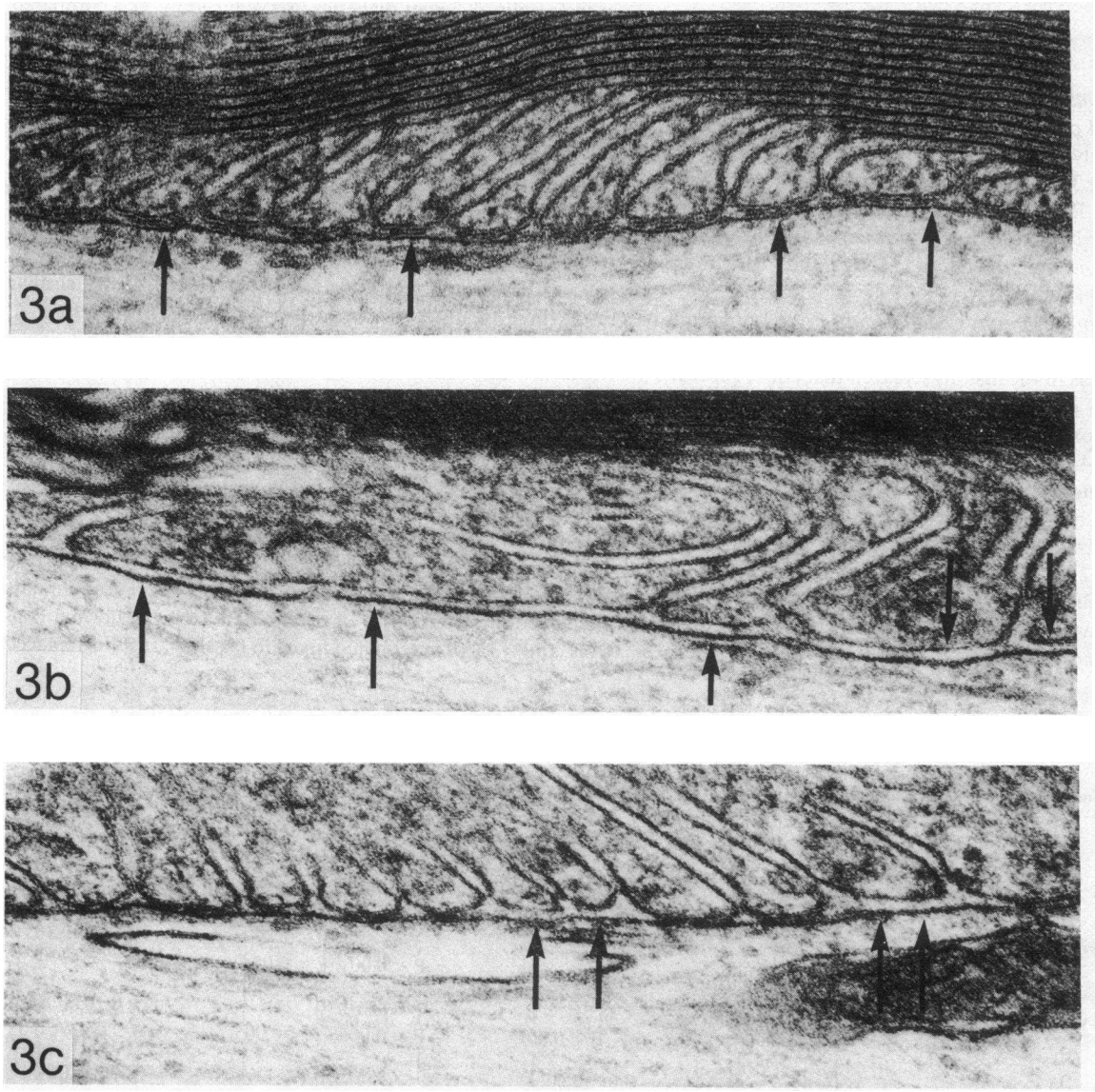

Figure 3. Effect of spontaneous diabetes and insulin replacement on axo-glial junctional complexes in paranodal terminal myelin loops of large myelinated axons from the sural nerve. Electronmicrographs compare terminal myelin loops from a nondiabetic control (*a*), an insulin-deficient diabetic (*b*), and an insulin-replaced diabetic (*c*). Regular junctional complexes between the axolemma and the terminal myelin loops are readily apparent in *a* (arrows), virtually absent in *b*, and present in reduced numbers in *c*. Quantitative differences in the frequency of terminal loops without junctional complexes (axo-glial dysjunction) are shown in Figs. 9 and 10. × 110,500.

Table IV. Effect of Prolonged Insulin Deficiency and Short-term Insulin Replacement on Sural Nerve Myelinated Fiber Morphometry

Animal group	Mean fiber area	Fiber number	Fiber density (fibers/mm²)	Fiber occupancy
	μm^2			%
Nondiabetic controls (n = 5)	36.6±1.0 ┐ P < 0.025	954±38	10,020±796	31.6±1.6
Insulin-deficient diabetics (n = 5)	31.4±1.3 ┘	897±69	11,560±871	33.8±1.9
Insulin-replaced diabetics (n = 5)	35.9±1.6	928±56	10,690±871	33.5±2.6
Baseline diabetics (n = 5)	34.9±1.4	971±28	10,570±866	36.5±2.9

Semi-thin (0.5 μm) toluidine-blue–stained cross-sections of the entire unifascicular sural nerve from five animals in each group were photographed at a magnification of 1,000 times, and used to calculate total fascicular area, total area, number, and density of myelinated nerve fibers as described in Methods.

a simultaneous decrease in the apparent frequency of large myelinated nerve fibers and an apparent increase in the frequency of small myelinated nerve fibers. Vigorous insulin replacement therapy increased large myelinated fibers without decreasing small myelinated fibers, which remained present in increased frequency (Fig. 5). Insulin-replaced diabetics differed from nondiabetic controls by a slightly but statistically significantly higher frequency of small myelinated fibers, whereas no difference was demonstrated in large-sized fibers (Fig. 6). Thus, the overall fiber size distribution in the insulin-replaced diabetic was significantly shifted toward larger fiber size with respect to the insulin-deficient diabetic ($P < 0.005$) (Fig. 5), but was barely shifted toward smaller fiber size with respect to the nondiabetic control ($P < 0.05$) on the basis of an apparent increase in the smallest myelinated fibers (Fig. 6). Mean fiber area was significantly reduced in the insulin-deficient diabetics compared with both the nondiabetic controls and the insulin-replaced diabetics (Table IV, column 1), and the slight difference between nondiabetic controls and insulin-replaced diabetics (Table IV, column 1) was attributable to the increase in small fibers (Fig. 6). Both the mean fiber area (Table IV, column 1) and the fiber caliber spectrum (Fig. 7) were similar in insulin-replaced rats at the completion of the study and in the insulin-deficient diabetics at baseline. Thus, insulin deficiency detectably increased the frequency of small myelinated nerve fibers during the first 12 wk of diabetes, and decreased the frequency of large myelinated nerve fibers between weeks 12 and 18; insulin replacement therapy from week 12–18 prevented the decrease in large myelinated fiber frequency without significantly altering the preexisting increase in small myelinated nerve fiber frequency. Since MNCV primarily reflects conduction in the largest population of myelinated motor fibers (22), the restoration of normal numbers of large myelinated nerve fibers in the insulin-replaced diabetics largely precludes a traditional morphometric explanation based on fiber caliber spectrum analysis for the persistently slowed MNCV in these animals.

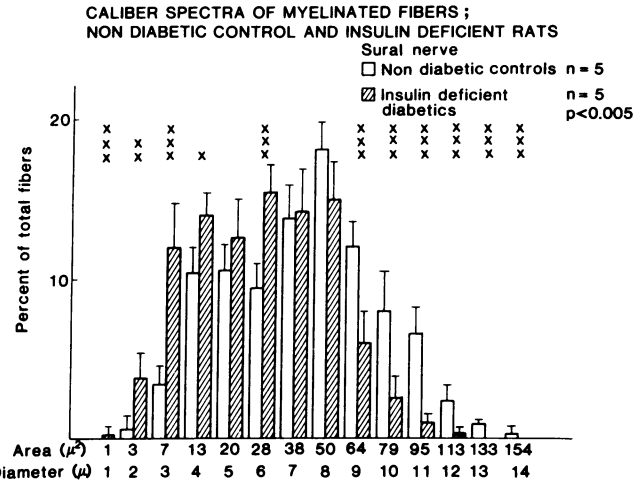

Figure 4. Effect of 18 wk of insulin deficient diabetes on sural nerve myelinated fiber caliber spectrum. Sural nerves from five insulin-deficient diabetics and five nondiabetic controls were fixed, embedded, and stained for light microscopy as described in Methods. Fiber diameters were calculated from computer-assisted measurements of fiber areas made at a magnification of 1,000 times, assuming that all fibers were round. The height of each bar represents the mean percentage of fibers within each increment in fiber area or diameter, and the error bar represents SEM. The overall P value in the upper right was determined by chi-square analysis, and the significance of difference for each fiber size is indicated by the symbols above each pair of bars as determined by t test analysis (x = $P < 0.01$; xx = $P < 0.005$; and xxx = $P < 0.001$).

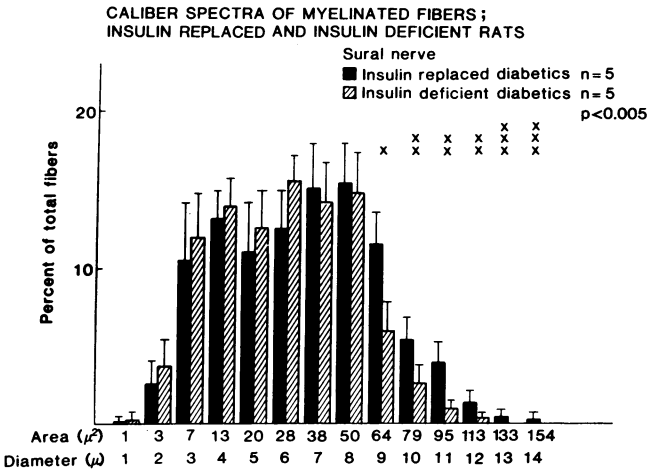

Figure 5. Effect of 6 wk of insulin replacement on sural nerve myelinated fiber caliber spectrum: comparison with 18-wk insulin-deficient diabetics. Insulin replacement increased the frequency of large myelinated fibers. Symbols and statistical analyses are as for Fig. 4.

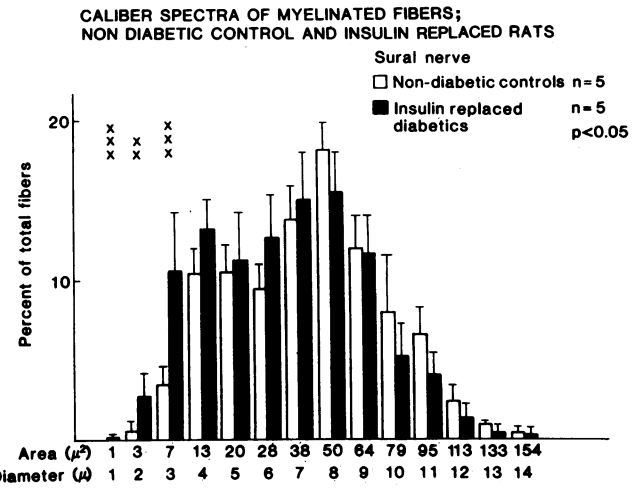

Figure 6. Effect of 12 wk of insulin deficiency followed by 6 wk of insulin replacement on sural nerve myelinated fiber caliber spectrum: comparison with nondiabetic controls. Statistical differences were confined to an increased frequency of smaller myelinated fibers in the insulin-deficient diabetics. Symbols and statistical analyses are as for Fig. 4.

Axon-myelin ratio (Fig. 8). Changes in the nerve fiber caliber spectrum can reflect either the appearance/disappearance of subpopulations of nerve fibers of differing diameters, or changes in the size of preexisting nerve fibers. The relationship between axonal cross-sectional area and the number of lamellae in the associated myelin sheath is expressed by the equation log nat (axonal area) = k × (number of myelin lamellae) (7, 23). When existing axons either shrink or swell, the number of myelin lamellae remains unchanged, thereby reflecting the preexisting axon size (7, 23, 24). Therefore, the axon-myelin ratio (k in the above equation and b in Fig. 8) is raised during axonal swelling or lowered during axonal shrinkage. The natural logarithms of individual axonal cross-sectional areas were plotted against the corresponding number of myelin lamellae for the four groups of animals studied (Fig. 8). The axon-myelin ratio (regression coefficient b in Fig. 8) was significantly decreased in insulin-deficient diabetics compared with both nondiabetic controls ($P < 0.01$) and insulin-replaced diabetics ($P < 0.025$) (Fig. 8). No differences in axon-myelin ratio were found between nondiabetic controls and insulin-replaced diabetics, or between insulin-replaced diabetics and baseline diabetic rats (Fig. 8). Thus axonal atrophy or shrinkage appears to have accounted for the decrease in myelinated fiber size that occurred in the insulin-deficient diabetics during the 6-wk study period (Fig. 4). Since the decrease in the axon-myelin ratio between weeks 12 and 18 of insulin deficiency was prevented by insulin replacement, fiber shrinkage cannot provide a structural basis for persistently slowed MNCV in the insulin-replaced diabetics.

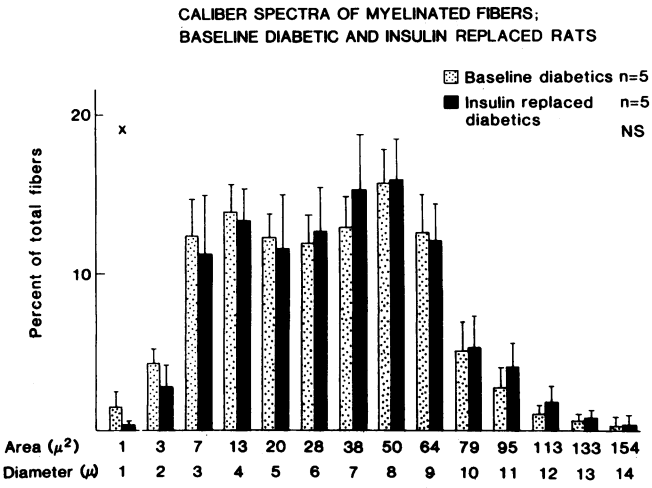

Figure 7. Effect of 6 wk of insulin replacement on sural nerve myelinated fiber caliber spectrum: comparison with baseline diabetics. Insulin replacement during the 6-wk protocol prevented the decrease in large myelinated fibers that occurs between weeks 12 and 18 in insulin-deficient diabetics (compare with Fig. 5). Symbols and statistical analyses are as for Fig. 4.

Axo-glial junctional complexes (Fig. 9). Terminal loops of myelin are normally attached to the axolemma by an array of junctional complexes that form a series of continuous circumferential bands around the axon in the paranodal region (25, 26). Intact axo-glial junctions were detected in 94±1.2% of paranodal terminal myelin loops in nondiabetic controls, 72.7±1.4% insulin-deficient diabetics, and 80.4±3.0% in insulin-replaced diabetics. The frequency of myelin loops without axo-glial junctions (i.e., axo-glial dysjunction) was significantly higher in the insulin-deficient diabetics than in both the nondiabetic controls ($P < 0.005$) and the insulin-replaced diabetics ($P < 0.025$). However, the frequency of axo-glial dysjunction remained greater in the insulin-replaced diabetics than in the nondiabetic controls ($P < 0.05$). Normal axo-glial junctions were found in 83.4±2.8% of terminal myelin loops in baseline diabetics, which was not significantly different from insulin-replaced animals. Thus, insulin replacement halted the loss of further axo-glial junctions between weeks 12 and 18 of insulin deficiency, but did not restore those junctions lost before week 12.

Terminal myelin loops with axo-glial dysjunction were most prominent in large myelinated fibers of both insulin-deficient and insulin-replaced diabetics. Since these large fibers more directly affect MNCV, the frequency of axo-glial dysjunction was plotted against nerve fiber diameter. A mean of 14.1±2.0 randomly selected fibers in each nerve were investigated in this way. The frequency of axo-glial dysjunction increased significantly with fiber size in insulin-deficient ($P < 0.005$) and insulin-replaced diabetics ($P < 0.05$) and in the baseline diabetics ($P < 0.05$), but not in the nondiabetic controls ($0.5 < P < 0.1$). This relationship differed significantly between nondiabetic controls and the three diabetic groups, and between the insulin-replaced and insulin-deficient diabetic groups; no differences in this relationship could be demonstrated between insulin-replaced diabetics and the baseline diabetics (Fig. 9).

Motor nerve conduction velocity and the frequency of axo-glial dysjunction were negatively correlated in the insulin-replaced diabetics and nondiabetic controls ($n = 10$, $r^2 = 0.87$, $P < 0.005$, slope = −0.41 m/s per % dysjunction) (Fig. 10). No such correlation was demonstrable in insulin-deficient diabetics at baseline or after the experimental treatment period ($n = 10$, $r^2 = 0.17$, $P > 0.1$, slope = −0.10 m/s per % dysjunction) (Fig. 10), where MNCV slowing correlates with (Na,K)-ATPase deficiency (15). Thus, MNCV slowing resistant to insulin replacement therapy that normalized nerve MI content, (Na,K)-ATPase activity, and fiber caliber spectrum was correlated and associated with a heretofore unrecognized axo-glial dysjunction in large myelinated nerve fibers in the chronically diabetic BB rat.

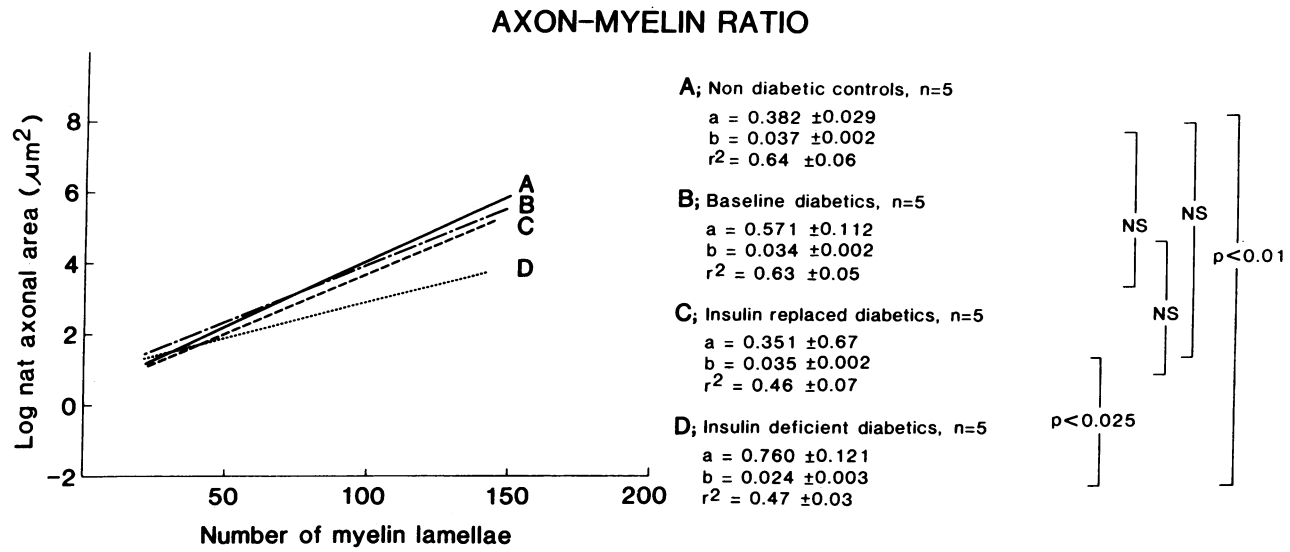

Figure 8. Effect of insulin deficiency and insulin replacement on axon-myelin ratio. The number of myelin lamellae around ~50 randomly chosen myelinated fibers in each sural nerve cross-section were counted at a magnification of 27,420 times, and compared with the natural logarithm of fiber area by linear regression analysis in each subgroup as described in Methods. A reduction in axonal area without a concomitant reduction in the number of myelin lamellae is indicated by a reduction in the axon-myelin ratio. Such axonal shrinkage appears to occur between weeks 12 and 18 of insulin deficiency, and is prevented by insulin replacement during this interval. a, intercept; b, slope; and r^2, coefficient of determination of linear regression. Significance of differences were calculated on the basis of slope.

Discussion

In diabetic human beings and animals, slowing of nerve conduction both precedes and accompanies the development of the neuroanatomical lesions characteristic of diabetic neuropathy (3, 27–29). The earliest detectable slowing of nerve conduction is readily reversible with metabolic intervention, and is attributed to reversible biochemical abnormalities in diabetic peripheral nerve (1–4, 29). With increasing duration of diabetes and/or the development of clinical signs and symptoms of diabetic neuropathy, nerve conduction slowing becomes less acutely responsive to metabolic intervention (30). In overt diabetic neuropathy, conduction slowing correlates primarily with loss of large myelinated nerve fibers, leaving only a small direct "metabolic" component of conduction slowing (27).

Although early biochemical defects are thought to contribute to the later development of less reversible structural and functional elements of diabetic neuropathy, the pathogenetic basis

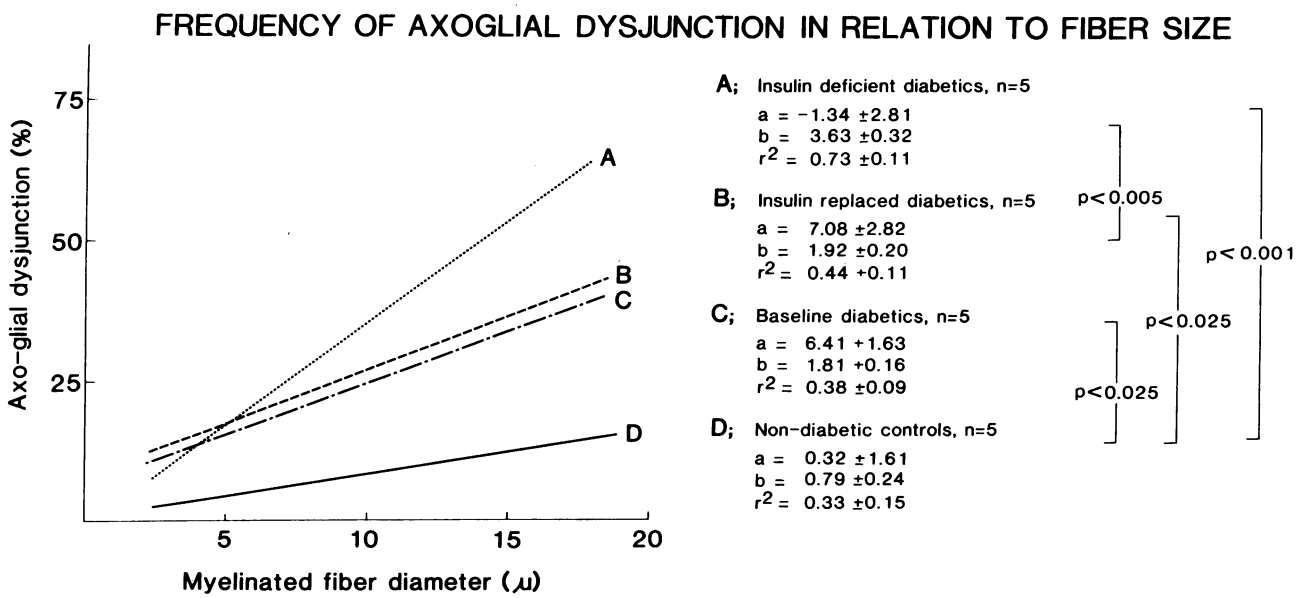

Figure 9. Effect of insulin deficiency and insulin replacement on the frequency of axo-glial dysjunction. The frequency of terminal myelin loops without morphologically demonstrable axo-glial junctional complexes (axo-glial dysjunction) was compared with myelinated fiber diameter by linear regression analysis as described in Methods for each of the four subgroups of rats. Symbols and statistical assessments are as for Fig. 8.

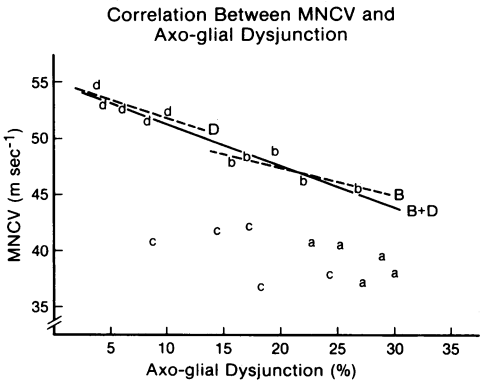

Figure 10. Relationship between MNCV and axo-glial dysjunction in nondiabetic controls (d), insulin-replaced diabetics (b), and insulin-deficient diabetics at baseline (c) and at the completion of the study (a). MNCV and axo-glial dysjunction were inversely correlated in the nondiabetic controls (D, $r^2 = 0.52$) and the insulin-replaced diabetics (B, $r^2 = 0.67$) that had normal nerve (Na,K)-ATPase activity (B + D, $r^2 = 0.87$, $P < 0.005$). No such correlation existed in the baseline (c) and insulin-deficient (a) rats, where slowed MNCV correlated with (and presumably reflected) reduced nerve (Na,K)-ATPase activity (15).

of this relationship is entirely unclear. Hyperglycemia in both man and animals produces a concentration-dependent conversion of glucose to sorbitol by the enzyme aldose reductase and an associated depletion of MI in nerve (31). Depletion of nerve MI in rodents in turn reduces nerve (Na,K)-ATPase activity (9, 14, 15), probably via a protein kinase C mechanism (16). (Na,K)-ATPase is thought to be localized primarily in the nodal and paranodal regions of large myelinated nerve fibers (32). Therefore, reduced axonal (Na,K)-ATPase activity is postulated to lead sequentially to the fourfold increase in axonal Na concentration, reduced axolemmal Na potential, subthreshold membrane potential, and selective conduction block of large myelinated fibers that diminishes MNCV and decreases evoked muscle

Pathophysiology of slowed conduction velocity during the metabolic phase

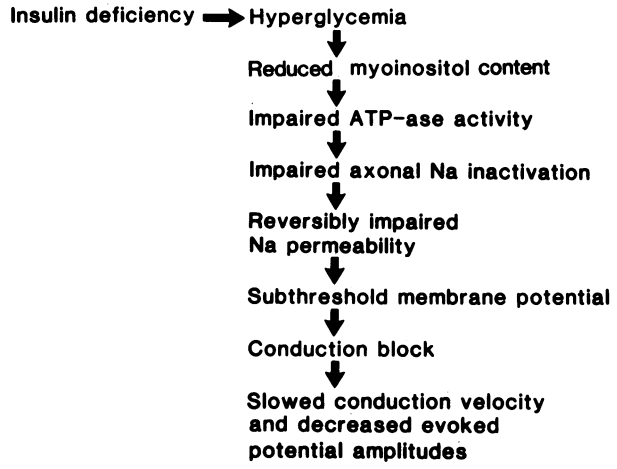

Figure 11. Proposed pathophysiological sequence responsible for early and rapidly reversible slowing of MNCV in the BB rat. See text for explanation.

potentials in the spontaneously diabetic BB rat (11). Diminished axolemmal Na potentials and increased intraaxonal Na levels in the first 4 wk of diabetes are accompanied by marked paranodal swelling in large myelinated axons (17) that is completely reversed by 2 wk of insulin replacement (17); these associated biochemical and structural findings give rise to a proposed pathogenetic sequence for early and reversible conduction slowing in the diabetic rat illustrated in Fig. 11.

In the present study, 6 wk of insulin replacement completely corrected the abnormalities in plasma glucose, osmolality, and pH; sciatic nerve MI content and (Na,K)-ATPase activity; sural nerve large fiber caliber spectrum; and tibial nerve EMPA produced by 12 wk of insulin deficiency. Tibial MNCV was only partially corrected, however. The complete correction of tibial EMPA militates against selective conduction block as the basis for residual tibial nerve conduction slowing, which therefore most likely reflects a true slowing of impulse conduction in individual nerve fibers (this is in contradistinction to the rapidly reversible phase of MNCV slowing in the BB rat that is attributable to a selective large-fiber conduction block [11]). Slowing of nerve conduction in chronic animal diabetes is generally ascribed to coexistent fiber atrophy since smaller diameter fibers conduct more slowly (22, 23). However, this mechanism cannot explain the residual conduction slowing in the insulin-replaced BB rat since large fiber atrophy, as assessed by fiber size frequency distribution, mean fiber size, and axon-myelin ratio, was completely prevented. The only remaining significant morphological and morphometric abnormalities in the insulin-replaced diabetics were increased malorientation of neurofilaments and the striking axo-glial dysjunction that was most prominent in large myelinated fibers.

Malorientation of neurofilaments alone is unlikely to lead to nerve conduction slowing (33), but may indicate impaired axoplasmic transport mechanisms (33–35) possibly related to either increased nonenzymatic glucosylation of tubulin (36) or alterations in axonal Ca metabolism (34). The persistence of maloriented neurofilaments after 6 wk of insulin replacement may reflect the slow turnover of these structures whose phagocytosis by Schwann cells may explain the honeycombed profiles at the Schwann cell-axon interface (28). Axo-glial dysjunction is a more likely cause of impaired conduction velocity. Axo-glial dysjunction was mostly confined to the large myelinated fibers that determine MNCV. Axo-glial junctional complexes comprise the transverse bands that bridge the intercellular gap between terminal myelin loops and the axolemma, and form the spiral arrays demonstrable in freeze fracture replicas of the paranodal axolemma (25, 26). These structures are thought to maintain the characteristically high density of axolemmal intramembraneous particles within the nodal area by limiting their lateral migration into the adjacent internodal regions. Since these intramembranous particles probably correspond to voltage sensitive Na channels, their depletion from the node as a result of axo-glial dysjunction may account for the reduced nodal Na-permeability and poorly reversible nerve conduction slowing in the chronically diabetic BB rat (Fig. 12) (26). This notion is further supported by the inverse correlation of MNCV and axo-glial dysjunction in the present study (Fig. 10).

The basis of the axo-glial dysjunction in rats replaced with insulin after 12 wk of diabetes has not been established. However, it may well represent persistent ultrastructural evidence of earlier paranodal swelling and its associated axo-glial spatial deformation (17). However, no loss of axo-glial junctions is demon-

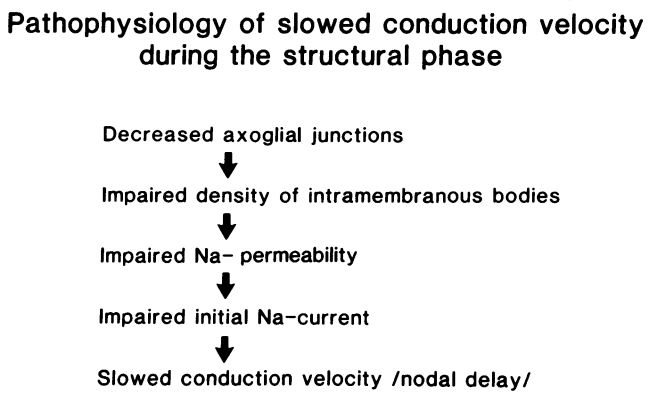

Figure 12. Proposed pathophysiological sequence responsible for later and poorly reversible slowing of MNCV in the BB rat. See text for explanation.

strable after 6 wk of diabetes when paranodal swelling is still prominent (17).

Alternatively, axo-glial dysjunction may reflect independent underlying biochemical abnormalities that may or may not be involved in the earlier reversible conduction slowing and paranodal swelling. Galactocerebroside, a lipid element in axo-glial junctions (37), is depleted from myelin isolated from the BB rat (38). Membrane glycolipids are further implicated in chronic conduction slowing by studies in the spontaneously diabetic db/db mouse, where ganglioside treatment selectively improves nerve conduction during the structural phase of diabetic neuropathy (39). Lastly, altered membrane phosphoinositide composition, and/or associated changes in protein kinase C activity and/or inositol-(1,4,5)-*tris*-phosphate-mediated Ca mobilization might directly influence the integrity of axo-glial junctional complexes (40), as might other abnormalities in the endoneurial extracellular environment in diabetes (41).

In summary, insulin deficiency initiates a series of metabolic alterations in diabetic peripheral nerve involving MI and the (Na,K)-ATPase, which can account for the early and reversible conduction block and paranodal swelling of large myelinated fibers in the BB rat. Continued insulin deficiency induces further poorly reversible structural damage, characterized by loss of axo-glial junctions, that probably accounts for the poorly reversible impairment of nerve conduction in the chronically diabetic BB rat. Whether more prolonged insulin replacement would reverse even these more persistent abnormalities, or whether prevention of the MI-related (Na,K)-ATPase defect would prevent or delay their occurrence, remain subjects for future investigation. However, the pathogenetic sequence proposed in Figs. 11 and 12 offers a potential theoretical framework by which to explain the progressive development of less readily reversible nerve dysfunction in human diabetic neuropathy. Furthermore, the BB rat may provide a useful animal model in which to test therapeutic interventions such as aldose reductase inhibitors and/or MI or ganglioside supplementation for their ability to prevent or treat various biochemical, functional, and structural phases or elements of diabetic neuropathy. Finally, diabetic neuropathy is classically characterized as a primary disorder of either the axon or the Schwann cell (42), whereas axo-glial dysjunction implies fundamental interactive abnormalities between both cell types in the region of the node of Ranvier.

Acknowledgments

The authors are indebted to Ms. M. Johnson, Mr. T. McEwen, and Mr. V. Nathaniel for their skillful technical assistance, and to Ms. M. Meunier and Ms. K. Willey for typing the manuscript.

This study was supported by grants from the Canadian Medical Research Council and the Canadian Diabetes Association, U. S. Public Health Service research grant RO1 29892, and the Harry Soffer Memorial Research Fund of the University of Pittsburgh.

References

1. Greene, D. A. 1983. Metabolic abnormalities in diabetic peripheral nerve: relationship to impaired function. *Metab. Clin. Exp.* 32:118–123.

2. Winegrad, A. I., D. A. Simmons, and D. B. Martin. 1983. Has one diabetic complication been explained? (editorial). *N. Engl. J. Med.* 308:152–154.

3. Gregersen, G. 1968. Variations in motor conduction velocity produced by acute changes of the metabolic state in diabetic patients. *Diabetologia.* 4:273–277.

4. Pietri, A., A. L. Ehle, and P. Raskin. 1980. Changes in nerve conduction velocity after six weeks of glucose regulation with portable insulin infusion pumps. *Diabetes.* 29:668–672.

5. Sima, A. A. F. 1984. Neuropathic and ocular complications in the BB-Wistar rat. *In* Lessons from Animal Diabetes. E. Shafrir and A. E. Renold, editors. John Libbey, London. 449–456.

6. Sima, A. A. F. 1983. The development and structural characterization of the neuropathies in the spontaneously diabetic BB-Wistar rat. *Metab. Clin. Exp.* 32:106–111.

7. Sima, A. A. F., M. Bouchier, and H. Christensen. 1983. Axonal atrophy in sensory nerves of the diabetic BB-Wistar rat. A possible early correlate of human diabetic neuropathy. *Ann. Neurol.* 13:264–272.

8. Greene, D. A., and S. A. Lattimer. 1982. Sodium and energy-dependent uptake of *myo*-inositol by rabbit peripheral nerve: competitive inhibition by glucose and lack of an insulin effect. *J. Clin. Invest.* 70: 1009–1018.

9. Greene, D. A., and S. A. Lattimer. 1983. Impaired rat sciatic nerve sodium-potassium ATPase in acute streptozocin diabetes and its correction by dietary *myo*-inositol supplementation. *J. Clin. Invest.* 72:1058–1063.

10. Brismar, T. 1983. Neuropathy-functional abnormalities in the BB-rat. *Metab. Clin. Exp.* 32:112–117.

11. Brismar, T., and A. A. F. Sima. 1981. Changes in nodal function in nerve fibers of the spontaneously diabetic BB-Wistar rat. Potential clamp analysis. *Acta Physiol. Scand.* 113:499–506.

12. Greene, D. A., and S. A. Lattimer. 1984. Action of sorbinil in diabetic peripheral nerve: relationship of polyol (sorbitol) pathway inhibition to a *myo*-inositol-mediated defect in sodium-potassium ATPase activity. *Diabetes.* 33:712–716.

13. Mayer, J. H., and D. R. Tomlinson. 1983. Prevention of defects of axonal transport and nerve conduction velocity by oral administration of *myo*-inositol or an aldose reductase inhibitor in streptozotocin-diabetic rats. *Diabetologia.* 25:433–438.

14. Greene, D. A., and S. A. Lattimer. 1983. A self-reinforcing metabolic defect in diabetic peripheral nerve involving *myo*-inositol and the sodium-potassium ATPase. *Clin. Res.* 31:387A. (Abstr.)

15. Greene, D. A., S. Yagihashi, S. A. Lattimer, and A. A. F. Sima. 1984. Nerve Na^+-K^+-ATPase, conduction and *myo*-inositol in the insulin-deficient BB-rat. *Am. J. Physiol.* 247:E534–E539.

16. Greene, D. A., and S. A. Lattimer. 1986. Protein Kinase C agonists acutely normalize decreased ouabain-inhibitable respiration in diabetic rabbit nerve. Implications for (Na,K)-ATPase regulation and diabetic complications. *Diabetes.* In press.

17. Sima, A. A. F., and T. Brismar. 1985. Reversible diabetic nerve dysfunction: structural correlates to electrophysiological abnormalities. *Ann. Neurol.* 18:21–29.

18. Sima, A. A. F. 1985. Annotation. Can the BB-rat help to unravel diabetic neuropathy? *Neuropathol. Appl. Neurobiol.* 11:253–264.

19. Sima, A. A. F., and K. Hay. 1981. Functional aspects and pathogenetic considerations of the neuropathy in the spontaneously diabetic BB-Wistar rat. *Neuropathol. Appl. Neurobiol.* 7:341–350.

20. Greene, D. A., P. V. DeJesus, and A. I. Winegrad. 1975. Effects of insulin and dietary myoinositol on impaired peripheral motor nerve conduction velocity in acute streptozotocin diabetes. *J. Clin. Invest.* 55: 1326–1336.

21. Yoda, A., and S. Yoda. 1980. A new simple method for NaK-ATPase rich membrane fragments. *Anal. Biochem.* 110:82–88.

22. Hursh, J. B. 1939. Conduction velocity and diameter of nerve fibers. *Am. J. Physiol.* 127:131–139.

23. Dyck, P. J., P. A. Low, M. F. Sparks, L. A. Hexum, and J. L. Karnes. 1980. Effect of serum hyperosmolality on morphometry of healthy human sural nerve. *J. Neuropathol. Exp. Neurol.* 39:285–295.

24. Dyck, P. J., E. H. Lambert, A. J. Windebank, A. D. Lais, M. F. Sparks, J. Karnes, W. R. Sherman, L. M. Hallcher, P. A. Low, and F. J. Service. 1981. Acute hyperosmolar hyperglycemia causes axonal shrinkage and reduced nerve conduction velocity. *Exp. Neurol.* 71:507–514.

25. Rosenbluth, J. 1978. Glial membrane specializations in extra paranodal regions. *J. Neurocytol.* 7:709–719.

26. Schnapp, B., and E. Mugnaini. 1978. Membrane architecture of myelinated fibers as seen by freeze-fracture. *In* Physiology and Pathobiology of Axons. S. G. Waxman, editor. Raven Press, New York. 83–123.

27. Behse, F., F. Buchtal, and F. E. Carlsen. 1977. Nerve biopsy and conduction studies in diabetic neuropathy. *J. Neurol. Neurosurg. Psychiatry.* 40:1072–1082.

28. Sima, A. A. F., A. C. Lorusso, and P. Thibert. 1982. Distal symmetric polyneuropathy in the spontaneously diabetic BB-Wistar rat. An ultrastructural and teased fiber study. *Acta Neuropathol. (Berl.).* 58:39–47.

29. Ward, J. D., C. G. Bowes, D. J. Fisher, J. Jessop, and R. W. R. Boher. 1971. Improvement in nerve conduction following treatment in newly diagnosed diabetics. *Lancet.* I:428–430.

30. Greene, D. A., M. J. Brown, S. N. Braunstein, S. S. Schwartz, A. K. Asbury, and A. I. Winegrad. 1981. Comparison of clinical course and sequential electrophysiological tests in diabetics with symptomatic polyneuropathy and its implications for clinical trials. *Diabetes.* 30:139–147.

31. Gillon, K. R. W., and J. N. Hawthorne. 1983. Sorbitol, inositol, and nerve conduction in diabetes. *Life Sci.* 32:1943–1947.

32. Odis, S. 1974. Systems of material transport in nerve fibers (axoplasmic transport) related to nerve function and trophic control. *Ann. NY Acad. Sci.* 228:202–223.

33. Griffin, J. W., and D. L. Price. 1981. Demyelination in experimental B,B'-iminodipropionitirile and hexacarbon neuropathies: evidence for an axonal influence. *Lab. Invest.* 45:130–141.

34. Odis, S. 1982. Calcium and the mechanism of axoplasmic transport. *In* Disorders of the Motor Unit. D. C. Schotland, editor. John Wiley & Sons, New York. 189–194.

35. Mendell, J. R., Z. Sahenk, J. R. Warmolts, J. K. Marshall, and P. Thibert. 1981. The spontaneously diabetic BB-Wistar rat. Morphologic and physiologic studies of peripheral nerve. *J. Neurol. Sci.* 52:103–115.

36. Williams, S. K., N. L. Howarth, J. J. Devenny, and M. W. Bilensky. 1982. Structural and functional consequences of increased tubulin glycosylation in diabetes mellitus. *Proc. Natl. Acad. Sci. USA.* 79:6546–6550.

37. Saida, K., T. Saida, H. Kayama, and H. Nishitani. 1984. Rapid alterations of the axon membrane in antibody-mediated demyelination. *Ann. Neurol.* 15:581–589.

38. Hofteig, J. H., K. S. Leon, A. J. Yates, and P. Thibert. 1983. Lipid abnormalities in nervous tissue of the diabetic BB-Wistar rat. *Neurochem. Path.* 1:265–277.

39. Norido, F., R. Canella, R. Zanoni, and A. Gorio. 1984. The development of diabetic neuropathy in the C57 BL/ks (db/db) mouse and its treatment with gangliosides. *Exp. Neurol.* 83:221–232.

40. Cahalan, M. 1978. Voltage clamp studies on the node of Ranvier. *In* Physiology and Pathobiology of Axons. S. G. Waxman, editor. Raven Press, New York. 155–168.

41. Tuck, R. R., J. D. Schmelzer, and P. A. Low. 1984. Endoneurial blood flow and oxygen tension in the sciatic nerves of rats with experimental diabetic neuropathy. *Brain.* 107:935–950.

42. Clements, R. S., Jr. 1979. Diabetic neuropathy—new concepts in its etiology. *Diabetes.* 28:604–611.